Metabotropic glutamate receptors activate dendritic calcium waves and TRPM channels which drive rhythmic respiratory patterns in mice

S. L. Mironov

DFG-Center of Molecular Physiology of the Brain, Department of Neuro- and Sensory Physiology, Georg-August-University, 37073 Göttingen, Germany

Respiration in vertebrates is generated by a compact network which is located in the lower brainstem but cellular mechanisms which underlie persistent oscillatory activity of the respiratory network are yet unknown. Using two-photon imaging and patch-clamp recordings in functional brainstem preparations of mice containing pre-Bötzinger complex (preBötC), we examined the actions of metabotropic glutamate receptors (mGluR1/5) on the respiratory patterns. The agonist DHPG potentiated and antagonist LY367385 depressed respiration-related activities. In the inspiratory neurons, we observed rhythmic activation of non-selective channels which had a conductance of 24 pS. Their activity was enhanced with membrane depolarization and after elevation of calcium from the cytoplasmic side of the membrane. They were activated by a non-hydrolysable PIP_2 analogue and blocked by flufenamate, ATP^{4-} and Gd^{3+}. All these properties correspond well to those of TRPM4 channels. Calcium imaging of functional slices revealed rhythmic transients in small clusters of neurons present in a network. Calcium transients in the soma were preceded by the waves in dendrites which were dependent on mGluR activation. Initiation and propagation of waves required calcium influx and calcium release from internal stores. Calcium waves activated TPRM4-like channels in the soma and promoted generation of inspiratory bursts. Simulations of activity of neurons communicated via dendritic calcium waves showed emerging activity within neuronal clusters and its synchronization between the clusters. The experimental and theoretical data provide a subcellular basis for a recently proposed group-pacemaker hypothesis and describe a novel mechanism of rhythm generation in neuronal networks.

(Received 28 November 2007; accepted after revision 26 February 2008; first published online 28 February 2008)
Corresponding author S. L. Mironov: DFG-Center of Molecular Physiology of the Brain, Department of Neuro- and Sensory Physiology, Georg-August-University, 37073 Göttingen, Germany. Email: smirono@gwdg.de

Mammalian breathing is generated in the lower brainstem (Rekling & Feldman, 1998; Richter & Spyer, 2001; Feldman & Del Negro, 2006). One of the brainstem regions involved in respiratory rhythmogenesis is the pre-Bötzinger complex (preBötC). Transverse slices of the rostral medulla oblongata (Smith *et al.* 1991) are capable of generating rhythmic discharges mediated by inspiratory interneurons which are coupled via glutamatergic synaptic connections. Despite considerable progress achieved in the last decade in understanding fundamental mechanisms responsible for generation and maintenance of breathing patterns, many issues regarding cellular mechanisms have remained to be addressed. Two basic questions still await their answers: what are the mechanisms which drive the activity of oscillators and how are such bursts synchronized within the preBötC.

Two models have been initially proposed to explain the respiratory rhythmogenesis. One assumes that intrinsic activity is generated within the soma (the pacemaker model), and another one proposes synaptic inhibition for the main mechanism responsible for establishment of the oscillatory activity within a network. Neither of the two models can fully account for all patterns of the respiratory network activity, and therefore they were first combined into a hybrid-pacemaker hypothesis, which was further modified to a group-pacemaker model and its main features have been summarized recently (Feldman & Del Negro, 2006). The group-pacemaker model proposes that a stable rhythm is generated through concerted short-range interactions between neurons and requires activation of Group I metabotropic glutamate receptors (mGluR1/5) and Ca^{2+}-sensitive channels of the transient

This paper has online supplemental material.

 DOI: 10.1113/jphysiol.2007.149021

receptor potential (melastonine) channels (TRPM) family. Pace *et al.* (2007) showed the burst-generating role of the Ca^{2+}-activated non-specific cationic current (I_{CAN}) in preBötC neurons, which they attributed to TRPM4 or TRPM5, which belong to the channels of the transient receptor potential (TRP) family which can be modulated by mGluR1/5 (Wissenbach *et al.* 2004). Then Crowder *et al.* (2007) demonstrated with RT-PCR that TRPM4 and TRPM5 mRNA are expressed in the preBötC and that the relevant TRPM4/TRPM5 modulation by phosphoinositides is an important determinant of burst-generating capabilities of preBötC neurons. Using neuron-specific transfection, we recently showed that neurons in the living respiratory network are organized in clusters (Hartelt *et al.* 2008). Such structure would fit a group-pacemaker hypothesis, but the static picture has to be complemented with the data about dynamical organization of the network.

Several channels have been proposed to drive oscillatory activity in the respiratory network. However, pharmacological blockade of ion channels which play an important role in other cell types such as hyperpolarization-activated I_h (Mironov *et al.* 2000; Thoby-Brisson *et al.* 2003), persistent Na^+ (Butera *et al.* 1999; Del Negro *et al.* 2002; Mironov & Langohr, 2005) and Ca^{2+}-dependent channels (Onimaru *et al.* 2003; Busselberg *et al.* 2003) either do not abolish the rhythm or it is re-established after activation of intracellular signalling pathways (Ruangkittisakul *et al.* 2006; Crowder *et al.* 2007).

The presence of oscillators is only necessary but not a sufficient condition for the appearance of oscillatory activity in a network (cf. Kuramoto, 2003; Strogatz, 2004; Newman *et al.* 2006 for recent surveys). For example, the classical Kuramoto model, which is often used to examine collective behaviour of ensembles of oscillators, predicts that their synchronization can occur only in a range of coupling parameters, otherwise the phases of oscillators are non-correlated.

Combining two-photon microscopy and patch-clamp recordings in the functional slice preparation, we focused on mGluR and the targets which they can activate. Previously we observed that various types of mGluRs differentially modulate single K_{ATP} and L-type Ca^{2+} channels (Ca_L) channels in the inspiratory network (Mironov & Richter, 2000*a*,*b*). Owing to the current interest in the role of mGluR in motor systems (Nistri *et al.* 2006), we further examined the actions of mGluR1/5 on other channels. Starting from the pharmacological evidence that mGluR1/5 and TRPM4-like channels are engaged in the generation of persistent motor output, we applied calcium imaging to monitor the activity of network by resolving single cells and their processes. We observed that rhythmic activity is generated in small clusters of neurons and it was related to spontaneous, mGluR1/5-dependent calcium waves in dendrites. The waves were initiated in dendrites and propagated towards the soma where they activated non-selective channels, and that led to subsequent generation of the burst of action potentials (AP). Conductance of channels, their voltage dependence and pharmacology conform to the properties of TRPM4 channels. Experimental data formed a basis of a model designed to describe neuronal activity in clusters of cells communicated through the calcium waves. Simulations showed synchronization of rhythmic activity within and between the clusters. The data obtained in '*in vivo*', '*in vitro*' and '*in silico*' are in line with a group-pacemaker hypothesis (Feldman & Del Negro, 2006) and describe specific subcellular mechanisms that can underlie its operation.

Methods

Preparation and two-photon imaging

All animals were housed, cared for and killed in accordance with the recommendations of the European Commission (No. L358, ISSN 0378-6978), and protocols were approved by the Committee for Animal Research, Göttingen University. 'Rhythmic' slices (thickness, 600 mm) containing a functional respiratory network (Smith *et al.* 1991) were prepared from brainstem of postnatal day (P) 5–12 NMRI mice as previously described (Mironov *et al.* 1998). After preparation, the slice was placed in the recording chamber on a nylon mesh, overlaid with a threaded home-made platinum–iridium 'horse-shoe' for mechanical stability and the neurons were visualized with infrared differential interference contrast (IR-DIC) illumination. Thirty minutes after the slice was positioned in the chamber, one hypoglossal (XII) rootlet was sucked into a blunt electrode for extracellular recordings of the respiratory motor output.

All experiments were made in oxygenated artificial cerebrospinal fluid (ACSF) which contained (mM): 128 NaCl, 3 KCl, 1.5 $CaCl_2$, 1.0 $MgSO_4$, 21 $NaHCO_3$, 0.5 NaH_2PO_4, 30 D-glucose, pH adjusted to 7.4 with NaOH, and was saturated with 95% O_2–5% CO_2 (carbogen). All chemicals were from Sigma (Deisenhofen), the receptor agonists and antagonists were from Tocris Cockson (Bristol, UK) and the fluorescent probes were from Molecular Probes (Leiden, the Netherlands). High-K^+ (45 mM) solution was prepared by exchanging Na^+ for K^+ and it was used as a standard tool to evoke membrane depolarization.

For calcium imaging, the slices were incubated with Fluo-3 AM for 30 min at 32°C in the dark, that was followed by a 30-min-long incubation in fresh medium to allow complete deesterification of the precursor dye. Before beginning the experiments, the slices were washed with fresh ACSF for 60 min. Experiments were performed at 32°C and ACSF was continuously aerated with carbogen.

Some experiments were performed also at 37°C and we did not observe the effects which might depend on temperature.

A custom-made two-photon laser scanning microscope (TPSM) (Müller *et al.* 2003), was used for imaging. It was composed of a modified upright microscope (Axioskop II, Zeiss) and a Ti–sapphire laser (Tsunami, Model 3941-M3BB, Spectra-Physics) pumped by a 5 W solid-state laser (Millenia Vs, Spectra-Physics). The laser was tunable in the range of 725–975 nm, delivering 200- to 220-fs-long laser pulses (duration determined at the specimen) at a frequency of 80 MHz. Average laser power was reduced by neutral grey filters (Linos Photonics) to 1–2 mW at the specimen. The illumination wavelength and pixel acquisition time were set to 800 nm and 7 μs, respectively. Software for system control and image acquisition was based on Labview (National Instruments) and IDL (Creaso) graphics surfaces. The imaging system was controlled by a MacIntosh G4 computer and scan mirrors were controlled by a subordinated VME computer. Although our facilities allow recordings of 3D data, the time resolution in such experiments is too low and we sought and examined the neurons whose dendritic trees were maximally depicted within a single focal plane.

Offline analysis was performed with Metamorph software (Princeton Instruments). Before analysis, the images were deconvoluted, background-subtracted and 3×3 median filtered as described (Hartelt *et al.* 2008). Time-dependent $[Ca^{2+}]_i$ changes were assessed as relative changes in fluorescence ($\Delta F/F_o$) and obtained either in regions of interest (ROI, $3\,\mu m \times 3\,\mu m$ in dendrites and $10\,\mu m \times 10\,\mu m$ in the soma) or by using line scans (width, $2\,\mu m$).

The time-course of fluorescence changes was used to establish the functional type of the cells by comparing their activity with respiratory motor output. The videos of representative experiments are presented in online Supplemental material. They demonstrate spontaneous calcium transients in slice preparation and in culture (Movies 1–4) and Movies 5 and 6 show the results of simulations. Each test in this study was repeated with at least four different preparations.

Cell culture

Respiratory neurons were isolated from neonatal mice as previously described (Mironov, 2006; Mironov & Symonchuk, 2006). Briefly, a 'standard rhythmic' slice (see above) was cut and, using a pipette with inner diameter of 400 μm, two symmetrically placed pre-Bötzinger complexes were isolated. After trypsin treatment, the dissociated cells were placed in a Neurobasal-A medium (Karlsruhe, Germany) onto poly L-lysine-coated glass coverslips. To abolish proliferation of glial cells, we added 5 μM cytosine arabinoside on the next day after plating. Cultures older than 3 DIV (days *in vitro*) were completely devoid of glia as verified by the absence of staining of GFAP (glial fibrillary acidic protein) During the experiments, the coverslips with cells were mounted in the recording chamber which was continuously superfused at 32°C with ACSF. The cultures were used at 4–21 DIV and each coverslip contained 1000–2000 cells.

Immunocytochemistry

GFAP staining was performed as described by Dr T. Manzke in his Thesis which can be downloaded from http://deposit.ddb.de/cgi-bin/dokserv?idn=97511106x&dok_var=d1&dok_ext=pdf&filename=97511106x.pdf. Labelling of NK-1 and μ-opioid receptors was performed as described for slices (Manzke *et al.* 2003; Hartelt *et al.* 2008) with minor modifications made for the use of cultured neurons. Briefly, the cells were fixed in 4% paraformaldehyde in phosphate-buffered saline (PBS), permeabilized with 0.5% Triton X-100 and non-specific binding was blocked with 2% bovine serum albumin (BSA) and 10% goat serum in PBS. Cells were incubated overnight in PBS containing the primary antibody at 1 : 400 dilution. After washing and blocking with 2% BSA and 2% goat serum in PBS, the cells were incubated for 2 h in the dark with appropriate secondary antibodies conjugated with Alexa 488 or Alexa 546. Immunofluorescence analysis was performed using a laser scanning confocal microscope (LSM 510; Zeiss).

Local drug application

In the experiments with preBötC neurons in culture, the drugs were locally applied as previously described (Mironov, 2006). To produce local changes in slices, we modified the application protocol and used a train of short pressure pulses (duration, 1–10 ms) at frequencies from 10 to 1 Hz. For establishing optimal parameters we calibrated application pipettes using ACSF solution containing 30 μM rhodamin (a brightly fluorescent dye). The pipette was positioned in a remote part of the slice and parameters of pressure pulses were adjusted to produce a fluorescence spot with a width $< 10\,\mu m$. Drug-containing application pipettes were positioned 3–4 μm from the object of interest, the soma or dendrite. Figure 1*A* shows that application of 0.1 mM Cd^{2+} about 100 μm away from the soma produced no changes in the amplitude of the whole-cell calcium currents, but when the perfusion pipette was placed in the vicinity of the soma, the application of Cd^{2+} produced fast block of I_{Ca}.

Electrophysiological and single channel analysis

Electrophysiological recordings were made in cells which showed rhythmic $[Ca^{2+}]_i$ changes in phase with the respiratory motor output. Patch electrodes of Kimax

capillary tubing (1.8 mm O.D.; American Scientific Products, Golden, CA, USA) were pulled on a two-stage List L/M-3P-A patch pipette puller (List Electronics, Darmstadt, Germany). The glass electrodes were used without heat-polishing and had 2–4 MΩ resistance. The approximate tip size was 2 μm. The pipette solution for all recordings contained (mM): 125 potassium gluconate, 10 NaCl, 2 $MgCl_2$, 10 Hepes, 0.5 Na_2ATP, pH adjusted to 7.4 with KOH. In inside-out recordings, the patches were excised into the bath solution which contained 1 mM EGTA and an appropriate amount of Ca^{2+} to adjust free calcium concentration in (sub)micromolar levels, which were calculated using free Web software (Winmaxc; Stanford University, Stanford, CA, USA). Thus, we added 0.9 and 1.1 mM $CaCl_2$ to Ca^{2+}-free ACSF with 1 mM EGTA to obtain, respectively, 0.3 and 10 μM free [Ca^{2+}]. The values were confirmed by measuring [Ca^{2+}] with a Ca^{2+}-sensitive electrode (InoLab, WTW Nova Analytics, Weilheim, Germany). ATP^{4-} specifically blocks TRPM channels (Nilius *et al.* 2005). To prepare micromolar solutions of ATP, we added 1 mM ATP to ACSF that contained 0.3 μM Ca^{2+}. According to Winmaxc, unbound ATP should correspond to 27 μM. Due to proton binding, the ATP^{4-} content is smaller and, according to Campbell *et al.* (1993), it should be 19 μM.

In recordings of whole-cell currents in the perforated-patch mode, 100 μg ml^{-1} nystatin was added to the pipette solution (Mironov *et al.* 1993; Mironov & Langohr, 2005) and the cells were clamped at −40 mV. Membrane currents were measured using an EPC-7 amplifier (ESF, Friedland, Germany) as previously described (Mironov *et al.* 1998). They were filtered at 3 kHz (−3 dB), digitized at 10 kHz, and stored for offline analysis. For an analysis of single channels, we first subtracted the action potentials from experimental records as previously described (Haller *et al.* 2001). Briefly, we generated a template by aligning and averaging of 50–100 single APs. Then the experimental trace was separated into episodes with overlapping ends. Using the mean-square-error criterium, the template was scaled to match experimental AP in each episode. After subtraction, the episodes were compiled into a continuous trace and, when the baseline showed slow variations, they were corrected. The open state probability values (P_{open}/N) were calculated by applying a moving average (window, 100 ms) of the mean current divided by the unitary current and the number of channels present, N. Single-channel conductance was obtained by measuring changes in single-channel current during the voltage ramp.

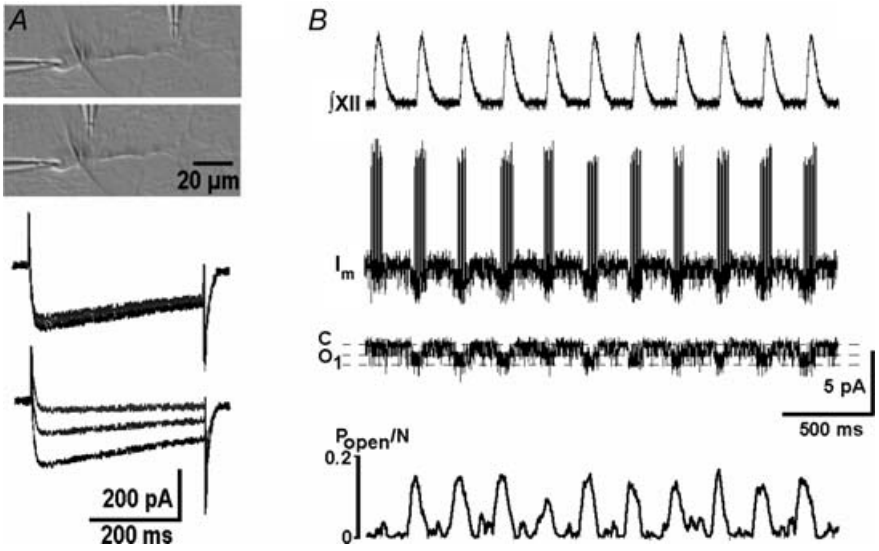

Figure 1. Experimental protocols applied in the present study
A, DIC image illustrating local applications in slices. The perfusion pipette was first placed over the dendrite in the vicinity of its branching point (as shown in top inset in the DIC image) and then repositioned close to the soma (the second image). Calcium currents (holding potential −60 mV, voltage steps to 0 mV) were measured before, 6 and 20 s after starting perfusion with 0.2 mM Cd^{2+}. Note the absence of effects when the pipette was about 60 μm away from the soma (three traces superimposed) and a decrease in current when the pipette was close to the soma. *B*, respiratory motor output (∫XII) and the membrane current (I_m). In this cell-attached configuration the action potentials were directed upward and channel openings were directed downward. The next trace shows the channel activity after APs were subtracted and the lowermost trace presents the mean open probability calculated as a moving average (window, 100 ms).

Modelling

In order to examine synchronization of neuronal activity in clusters, we considered an ensemble of 'excitability' sites capable of generating spontaneous calcium transients that propagated along dendrites to neurons and elicited subthreshold changes in membrane potential (V_m). For determining time-dependent changes in free cytoplasmic Ca^{2+} (C) at the nth site, a simple model of the Ca^{2+}-induced Ca^{2+} release (CICR) was used. It consisted of two equations (Mironov, 1990; Mironov, 1994):

$$\frac{dC_n}{dt} = P\frac{\theta_n^2 C_n^2}{(C_n+K)^2} + V_{max}\frac{C_n^2}{(C_n+K')^2} + J_{Ca} + \sum{}' C_m(t-\tau)$$

$$\frac{d\theta_n}{dt} = \alpha(1-\theta_n) - \beta\theta_n C_n \quad (1)$$

The first equation describes the Ca^{2+} release (dissociation constant $K = 0.2\ \mu$M, permeability of release channels, $P = 10\ \mu\text{M s}^{-1}$), Ca^{2+} removal from the cytoplasm by SERCA (dissociation constant $K' = 0.1\ \mu$M, maximal velocity $V_{max} = 2\ \mu\text{M s}^{-1}$), and the Ca^{2+} influx into the cell ($J_{Ca} = 0.001\ \mu\text{M s}^{-1}$). The second equation describes desensitization of Ca^{2+} release and thus defined whether the site was in the refractory state. The process was represented by a first-order reaction with the rate constants $\alpha = 3\ \text{s}^{-1}$ and $\beta = 4\ \text{s}^{-1}\ \mu\text{M}^{-1}$. The last sum in the first equation described the interactions between the sites through the calcium waves. As in our experiments the waves propagated at about constant velocity, we did not consider them explicitly and assumed that one site 'sees' changes in $[Ca^{2+}]$ at the adjacent site after a certain time (delay, τ). For the mean velocity of the $[Ca^{2+}]$ wave ($72\ \mu\text{m s}^{-1}$) (Fig. 5) and the mean distance between the sites ($45\ \mu$m) (Fig. 3), the delay is about 0.6 s.

In order to determine changes in V_m caused by $[Ca^{2+}]_i$ transients, we used the current balance equation

$$C_m dV_m/dt = I_{leak} + I_{TRPM} \quad (2)$$

with chord conductances

$$I_{leak} = g_{leak}(V_m - V_{baseline})$$

$$I_{TRPM} = g_{TRPM} V_m [Ca^{2+}]^5/(K_{TRPM} + [Ca^{2+}])^5 \quad (3)$$

where the membrane capacitance $C_m = 40$ pF, $g_{leak} = 2.5$ nS, $g_{TRPM} = 25$ nS and $V_{baseline} = -65$ mV. The last term in eqn (3) describes activation of channels by Ca^{2+} according to the apparent dissociation constant $K_{TRPM} = 1\ \mu$M (Prawitt *et al.* 2003). In simulations, the neurons were placed between 'excitability' sites. APs were not considered explicitly and it was assumed that the burst starts when V_m crosses a threshold of -50 mV (Rekling & Feldman, 1998; Richter & Spyer, 2001; Feldman & Del Negro, 2006). Previous studies (Mironov, 1983) showed that omission of voltage-dependent conductances which are involved in AP generation do not modify the conclusions reached in considering only subthreshold V_m changes. Simulations were made by programming eqns (1)–(3) using Turbo-Pascal 7.0, which were numerically solved using the fourth-order Runge–Kutta algorithm with a step size of 0.01 s.

Abbreviations

ACSF, artificial cerebrospinal fluid; AP, action potential; $[Ca^{2+}]_i$, intracellular free Ca^{2+} concentration; CICR, Ca^{2+}-induced Ca^{2+} release; CNQX, 6-cyano-7-nitroquinoxaline-2,3-dione; DIC, differential interference contrast; DiC_8PIP_2, phosphatidylinositol(3,4) bisphosphate DiC_8; DHPG, (*S*)-3,5-dihydroxyphenylglycine; DIV, days *in vitro*; ER, endoplasmic reticulum; LY367385, (+)-2-methyl-4-carboxyphenylglycine; *N*, number of active channels; preBötC, pre-Bötzinger complex; P_{open}, open probability of the channels; ROI, regions of interest; TRPM, transient receptor potential (melastonine) channels; TPSM, two-photon scanning microscopy.

Results

mGluR1/5 and TRPM4-like channels in the respiratory network in slice preparation

Figure 2 shows the effects of a group I mGluR agonist (DHPG) and antagonist (LY367385) on the respiratory motor output and inspiratory drive currents. The effects of DHPG were dependent on the drug concentrations used: 5 μM DHPG augmented inspiratory drive currents and the frequency and amplitude of the inspiratory bursts significantly increased from 8.2 ± 0.5 to $11.8 \pm 0.6\ \text{min}^{-1}$ and from 35 ± 4 to 52 ± 5 pA, respectively ($P < 0.05$, $n = 4$, Fig. 2). In another four slices examined, 50 μM DHPG transiently potentiated inspiratory bursts followed by their depression. In both cases, the activity was restored but remained augmented after washing out the drug, corresponded to about a 20% increase in the frequency and amplitude of the bursts. The effects persisted for about 1 h after the drug was washed out. The actions of DHPG at both concentrations were not observed in the presence of 200 μM LY367385 (examined in three different slices for both 5 μM and 50 μM DHPG). LY367385 at 50 μM significantly slowed down the rhythm from 8.4 ± 0.6 to $6.1 \pm 0.5\ \text{min}^{-1}$ and decreased the amplitude of the inspiratory drive currents by $35 \pm 7\%$ ($P < 0.05$, $n = 4$, Fig. 2). The activity was restored after wash-out, but the rhythm remained slightly suppressed for about 1 h.

mGluRs are differentially coupled to various channels and receptors that play an important role in functioning of various motor systems (Nistri *et al.* 2006). Group I mGluRs have been recently implicated in activation of TRPM4-like channels in the respiratory network (Pace *et al.* 2007) and RT-PCR analysis revealed TRPM4/5 channels in preBötC (Crowder *et al.* 2007). The role of TRPM-like channels was first examined by applying gadolinium (Gd^{3+}), a trivalent lanthanide, which has emerged as the most commonly used tool to identify phenomena dependent on stretch-activated channels (Hamill & McBride, 1996), and Gd^{3+} has also been used as a blocker of channels of the TRP family (Kraft & Harteneck, 2005; Ramsey *et al.* 2006; Nilius *et al.* 2007). Gd^{3+} at 30 μM specifically blocks TRPM4 channels (Morita *et al.* 2007) and at this concentration we observed reversible suppression of both respiratory motor output and inspiratory drive currents ($n = 5$, Fig. 2, last trace).

In order to further examine the role of TRPM channels in respiratory activity, we sought for a functional expression of these channels using single-channel recordings. Channel activity was recorded in 187 cell-attached patches from 202 inspiratory neurons examined in 58 different slices. Usually two identical channels were present in the patch (only 5% of recordings showed single openings, and 12% contained three channels). When the pipette solution contained 30 μM Gd^{3+}, no channel activity was observed ($n = 12$). Application of negative pressure to the patch pipette (Morita *et al.* 2007) stimulated the activity of the channels (Fig. 3*A*). The open probability P_{open}/N increased from 0.08 ± 0.02 to 0.32 ± 0.04 ($P < 0.05$, $n = 4$, Fig. 3*B*). The channel activity was retained after the patch was excised and, in the inside-out patches, the channels were no longer activated by negative pressure ($n = 4$, data not shown), which resembles the behaviour of TPRM4 channels in myocytes (Morita *et al.* 2007).

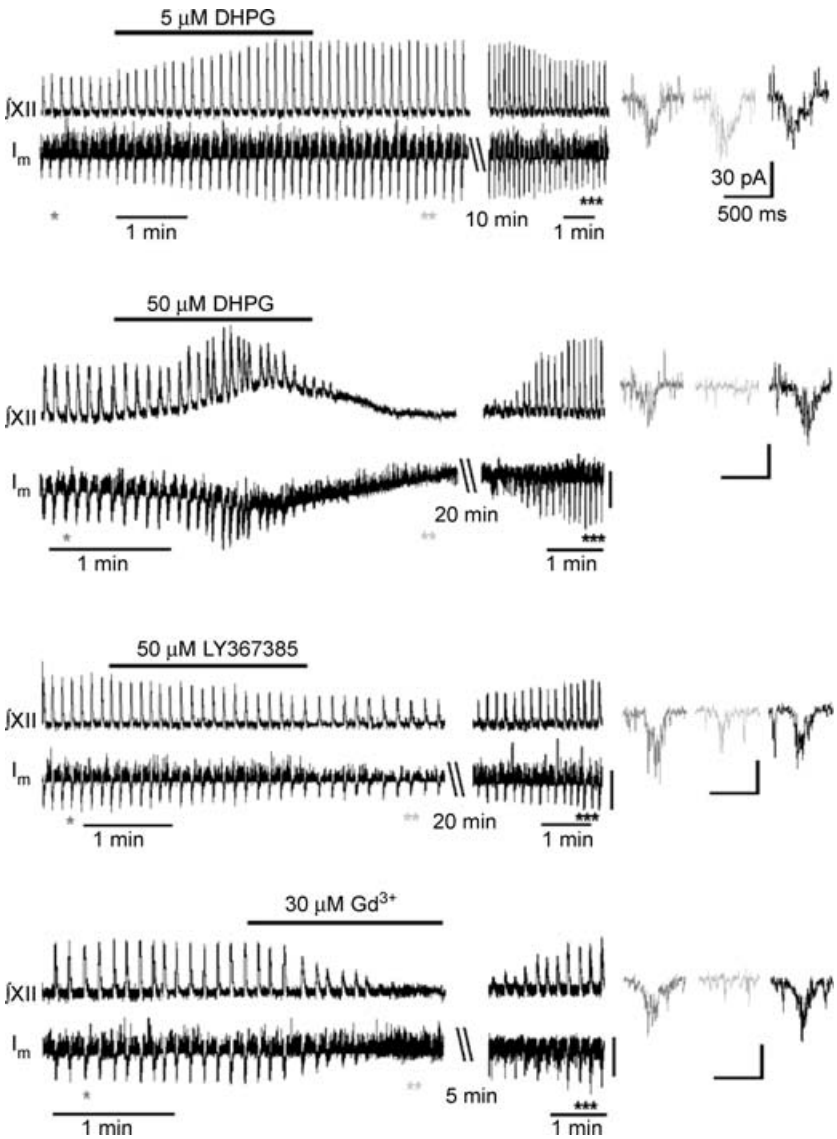

Figure 2. Group I metabotropic glutamate receptors in the respiratory network
Traces in left panel show the actions of mGluR1/5 agonist (DHPG), antagonist (LY367385), and Gd^{3+} (applied to block TRPM4-like channels) on the respiratory motor output ($\int$XII) and membrane current (I_m) recorded in the inspiratory neurons in the perforated patch-clamp mode (holding potential, −40 mV). The drugs were washed out for the periods indicated, and the initial activity was restored (note the compressed time-scale in the presentation). The episodes indicated by asterisks in the I_m trace show inspiratory drive currents at the expanded time-scale of the right.

Mean channel conductance in inside-out patches was 24 pS which is close to that reported for Ca^{2+}-activated non-specific cationic (CAN) channels (Cho *et al.* 2003) and TRPM4/5 channels (Kraft & Harteneck, 2005; Ramsey *et al.* 2006; Nilius *et al.* 2007). The same conductance was measured in cell-attached patches ($n = 12$, data not shown). Channel activity increased with membrane depolarization and P_{open} showed sigmoidal dependence on the patch membrane potential, similar to that observed in other cell types (Prawitt *et al.* 2003; Morita *et al.* 2007). We examined also pharmacological properties of the channels. Using low-Ca^{2+} ACSF, which contained

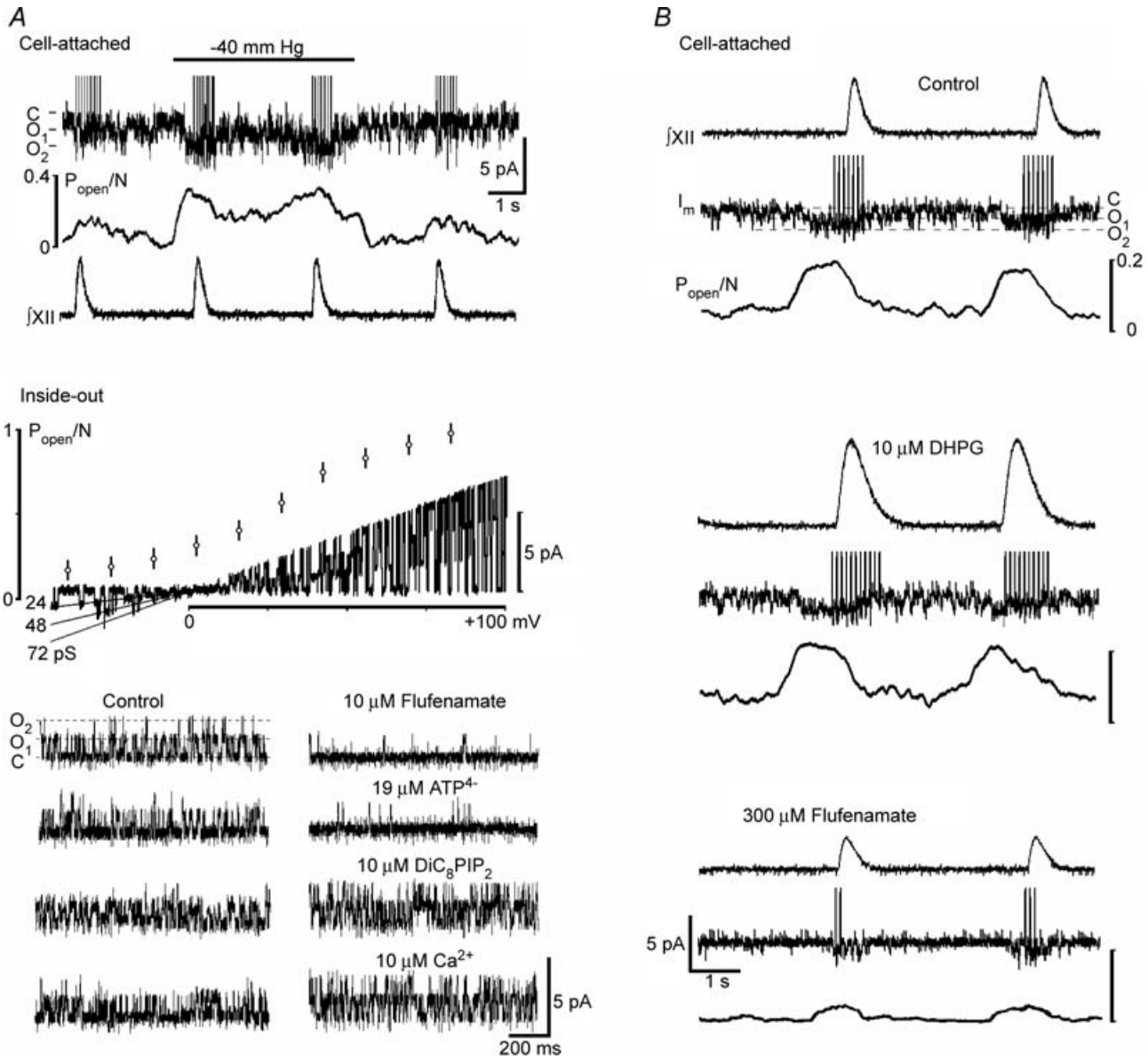

Figure 3. TRPM4-like channels in the inspiratory neurons and their modulation
A, first panel shows potentiation of channel activity during application of negative pressure to the cell-attached patch. The two panels below present *I–V* relationship and modulation of channel activity in the inside-out patches in bath solution contained 0.3 μM Ca^{2+}. The middle panel shows open channel probability at different potentials (mean ± S.E.M.) and changes in single-channel current during the voltage-ramp that correspond to the mean channel conductance 24 pS. Application of 10 μM flufenamate and 19 μM ATP^{4-} to the cytoplasmic side inhibited channel activity (holding potential, +50 mV), and it was augmented 2 min after addition of 10 μM non-hydrolysable DiC_8PIP_2 or 10 μM Ca^{2+} to the bathing solution. *B*, representative recordings show the activity of TRPM4-like channels in cell-attached patches in the control, 2 min after addition of 10 μM DHPG to the bath, and 10 min after subsequent addition of 300 μM flufenamate. Note differences in acting concentrations of flufenamate in inside-out and cell-attached patches that indicate its intracellular action.

0.3 μM Ca^{2+}, as a control, we observed that 10 μM flufenamate, a commonly used CAN channel blocker (Cho *et al.* 2003; Pace *et al.* 2007), decreased the activity of the channels (P_{open}/N decreased from 0.15 ± 0.03 to 0.02 ± 0.01, $P < 0.05$; $n = 4$). We also used ATP^{4-}, which selectively blocks TRPM4 channels at micromolar concentrations and has no effect on TRPM5 channels up to 1 mM (Nilius *et al.* 2005). Application of 19 μM ATP^{4-} (see Methods) decreased P_{open}/N from 0.17 ± 0.04 to 0.01 ± 0.01 ($P < 0.05$; $n = 3$). The channels were activated after application of 10 μM Ca^{2+} to the cytoplasmic side (P_{open}/N increased from 0.19 ± 0.03 to 0.62 ± 0.06, $P < 0.01$; $n = 4$) and 10 μM of the non-hydrolysable PIP_2 analogue DiC_8PIP_2 (P_{open}/N increased from 0.17 ± 0.04 to 0.45 ± 0.07, $P < 0.05$; $n = 3$).

During the respiratory cycle, the activity of the channels transiently increased just before the inspiratory burst appeared (Fig. 3*B*). In the presence of 10 μM DHPG, the maximal P_{open} and burst duration were augmented by $31 \pm 7\%$ and $51 \pm 8\%$ ($P < 0.05$; $n = 4$). Flufenamate (300 μM) suppressed these variables by $76 \pm 7\%$ and $62 \pm 9\%$ ($P < 0.05$; $n = 4$, Fig. 3*B*). In comparison with inside-out patches, the effects of flufenamate in cell-attached patches developed slowly and the steady state was attained about 10 min after applying the drug to the slice. This can be explained by a cytoplasmic site of action of flufenamate (Cho *et al.* 2003), which is a bulky polar molecule and has poor membrane permeability.

Respiration-related activity as revealed by calcium transients in slice preparation

Previous studies in preBötC-containing slices (Koshiya & Smith, 1999; Mironov & Langohr, 2005; Thoby-Brisson *et al.* 2005) and organotypic cultures (Baker *et al.* 1995) have documented spontaneous calcium transients in single inspiratory neurons. Using calcium transients as indicators of single cell activity (Supplementary Movie 1), we presented the peak times of each transient as rasterplots (Fig. 4*A*). The data indicated prominent peaks

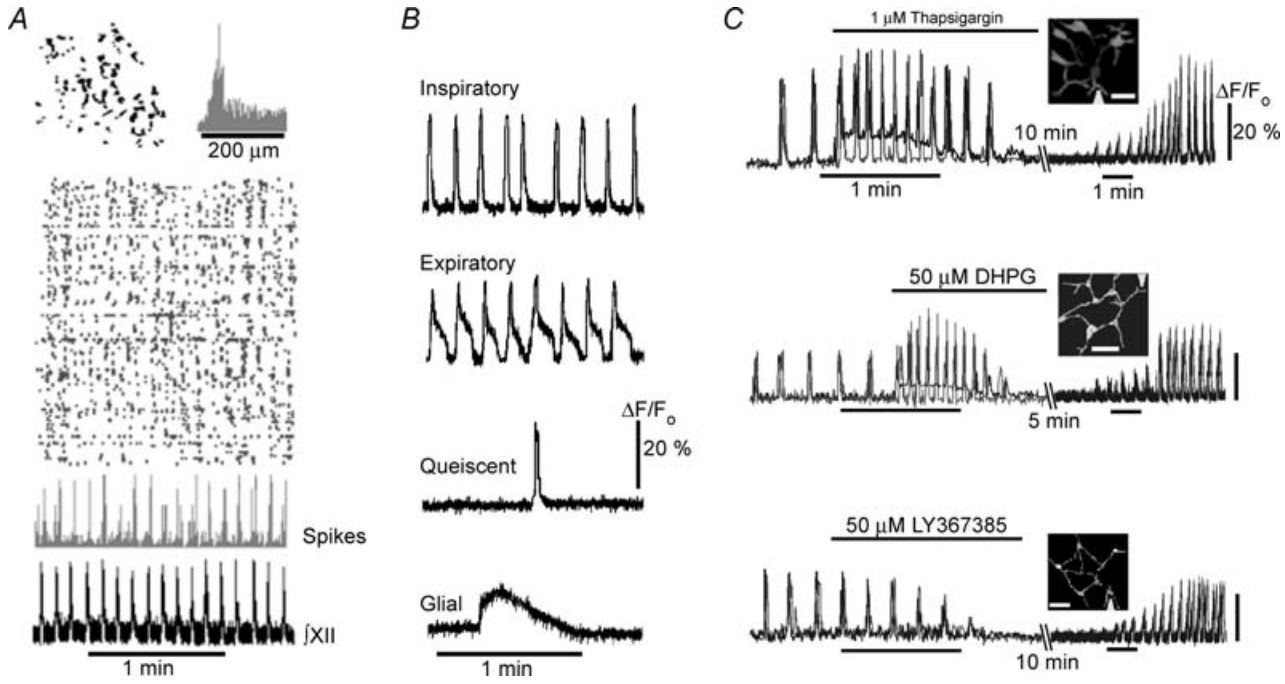

Figure 4. Two-photon $[Ca^{2+}]_i$ imaging of persistent oscillatory activity in respiratory neurons
A, spatial and temporal correlations of the rhythmic cell activity in the functionally intact preparation. Top left inset shows representative distribution of active cells in a network and the right inset presents the histogram of distances between them. In the rasterplot below each row corresponds to a single cell, and each mark to a detected $[Ca^{2+}]_i$ transient. A histogram below gives the number of cells active at each frame recorded that correlates with the respiratory motor output in the lowermost trace. A sample trial is presented in Supplementary Movie 1. *B*, main types of spontaneous transients in slices. *C*, spontaneous activity in clusters of neurons in the functional slice preparation and its modulation. The insets in each panel show halftone images of neuronal clusters and the triangles at image borders indicate the positions of perfusion pipette for drug applications. Scale bars in all insets, 20 μm. The traces were obtained in dendrites (black curves) and in the soma of neurons (grey curves). All effects were reversible and the activity was restored after the drug was washed out (restoration of activity took different times and it is presented at the compressed time scale). The first experiment with thapsigargin is also presented in Supplementary Movie 2.

of synchronous activity characteristic of slow oscillations (0.15 ± 0.02 Hz), which correlated with respiratory motor output (Fig. 4*A*, 124 movies analysed). All spontaneous events were blocked by bath application of the Na^+ channel blocker tetrodotoxin (0.3 μM) and the AMPA receptor antagonist CNQX (10 μM). On the basis of single-cell activity, we distinguished between the inspiratory neurons ($48 \pm 5\%$ of all active cells) which discharged in phase with respiratory motor output, expiratory neurons ($8 \pm 3\%$) which were active after the peak of synchrony and quiescent cells ($44 \pm 4\%$) which generated occasional transients not related to respiratory motor output (Fig. 4*A*). We noticed that the activity was localized within clusters which consisted of six to nine cells and all of them demonstrated synchronous activity (Supplementary Movie 1). Mean nearest-neighbour distance within the clusters was 45 ± 12 μm (12 slices examined) as represented by the maximum in the histogram of interneuronal distances (Fig. 4*A*).

Spontaneous activity of neurons in clusters was dependent on mGluR1/5. Local perfusion of dendrites with DHPG and LY367385 elicited effects (Fig. 4*B*), which were similar to those observed for the inspiratory drive currents and respiratory motor output (Fig. 2*B*). Local application of thapsigargin, a SERCA inhibitor which depletes internal Ca^{2+} stores, mimicked the effects of 50 μM DHPG. In these experiments, all drugs were applied locally (estimated application width < 10 μm, see Methods), but the activities of all neurons in a cluster were modulated, indicating exchange of information between the cells (this notion is further supported by the experimental and modelling data presented in Figs 6 and 7).

Spontaneous calcium transients in cultured preBötC neurons

Medullary organotypic cultures of newborn rats generate rhythmic activity (Baker *et al.* 1995). We asked whether pre-BötC neurons have an intrinsic activity and prepared a primary cell culture devoid of glial cells. Pre-BötC neurons expressed neurokinin (NK-1), opioid (μOR) and serotonin (5-HT-4a) receptors (Fig. 5*A* and *B*), which are proposed as markers of inspiratory neurons (Gray *et al.* 1999; Guyenet & Wang, 2001; Manzke *et al.* 2003; McKay *et al.* 2005). Proportions of cells which contained NK-1, mOR and 5-HT-4a receptors were similar to those measured in slice preparations (Manzke *et al.* 2003; see also Supplement 1). In primary culture, preBötC neurons often formed clusters (Fig. 5) composed of several neurons which all generated rhythmic calcium transients (Fig. 5*D* and Supplementary Movie 3). Rhythmic activity disappeared after blockade of synaptic activity (Supplement 1). The neurons without apparent connections to other cells, showed no spontaneous activity. Voltage-clamp recordings in rhythmically active cells demonstrated inspiratory drive currents (Fig. 5*E*) which resembled those observed in the functional slice preparation (Fig. 2). The data obtained in primary culture indicate that clusters of neurons can represent a functional unit capable of generating rhythmic activity, indicating no acute necessity of glial cells and synaptic inhibition for rhythm generation.

Calcium waves in dendrites and their relation to the inspiratory activity in slice preparation

Spontaneous activity in the functional slice preparation was related to the calcium waves in dendrites. They often appeared close to the dendritic branching points and propagated towards the soma (Fig. 6*A*; Supplementary Movie 4). Using measured calcium profiles, we estimated the mean wave velocity as 72 ± 12 μm s^{-1} ($n = 6$). In many neurons (Larkum *et al.* 2003; Augustine *et al.* 2003; Hagenston *et al.* 2008), the propagation of Ca^{2+} waves is supported by Ca^{2+}-induced Ca^{2+} release (CICR) from internal stores. The measured speed agrees with values which were obtained in other neurons (reviewed by Augustine *et al.* 2003) and with theoretical estimates

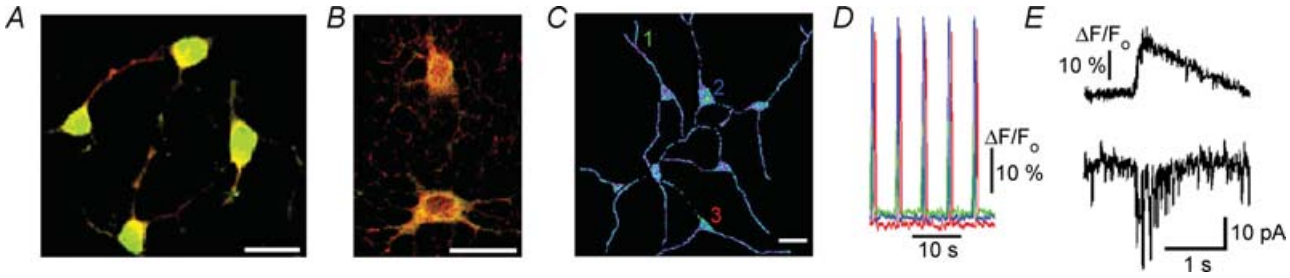

Figure 5. preBötC neurons in primary culture
A, staining for 5-HT-4a receptors (green) and MAP2 (red). *B*, staining for NK-1 (green) and μ-opioid receptors (red). *C*, cluster of active respiratory neurons. *D*, calcium changes. Multicoloured traces correspond to ROIs indicated in *C*. A sample trial is presented in Supplementary Movie 3. *E*, calcium transients in the cell soma and membrane current measured at the holding potential −40 mV. Scale bars in all panels, 20 μm.

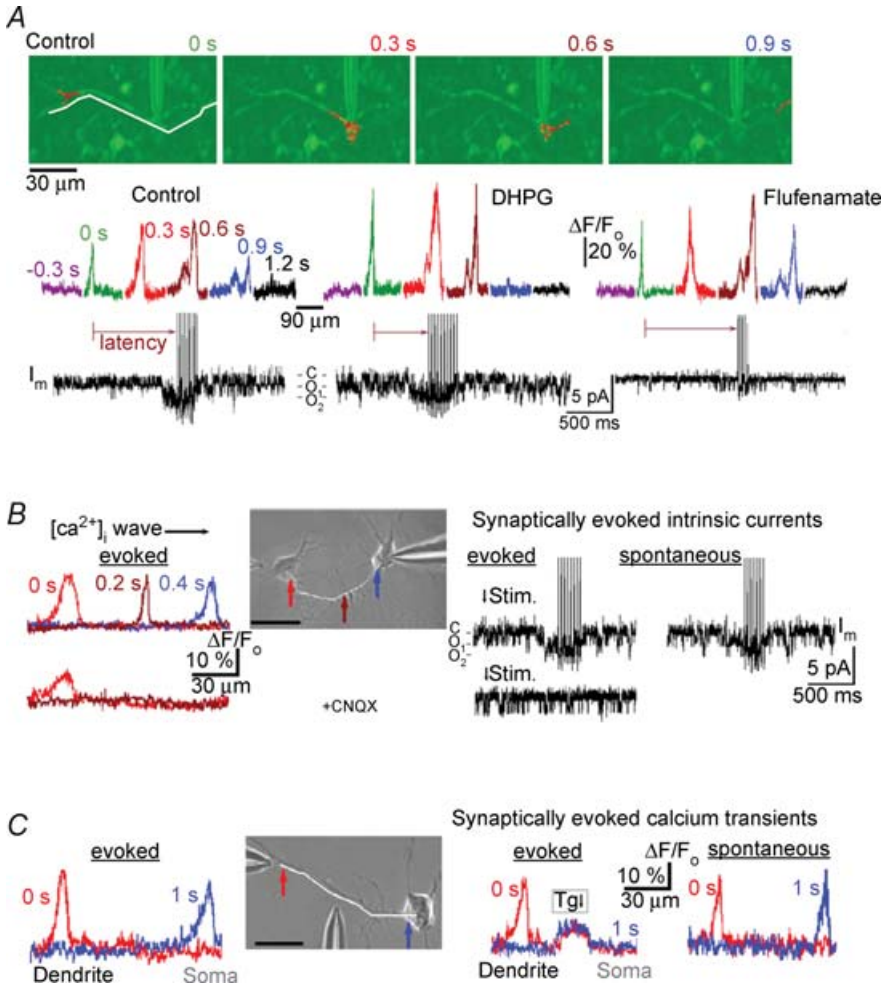

Figure 6. Correlation between bursting activity and calcium waves
A, calcium waves, bursting and channel activity in the functionally intact preparation. Top, overlay of fluo-3 fluorescence (red, sampling interval, 0.3 s) and DIC image (green). The fluorescence scans below were obtained along curvilinear path as indicated by the white line in the first frame. Time counts begin from the appearance of the wave in dendrite and differently coloured profiles are positioned above respective parts of the cell-attached patch-clamp recordings. Note that the calcium wave first appeared at the dendritic branching point, propagated across the soma and invaded the opposite dendrite. Distances between the wave fronts corresponded to the mean wave velocity, 72 μm s^{-1}. A sample trial is presented in Supplementary Movie 4. Note an increase in channel activity when the wave arrived at the soma after which the burst of action potentials was generated. After control measurements, 5 μM DHPG was added to the bath to activate metabotropic glutamate receptors and 2 min after, the recordings were made. Note that in the presence of DHPG, the wave propagated faster (the velocity increased to 100 μm s^{-1}) and the burst lasted longer. The next recording was made 10 min after DHPG was washed out with a fresh solution containing 300 μM flufenamate. The wave velocity (72 μm s^{-1}) was similar to that in the control, but the activity of the channels significantly diminished and the burst duration was much reduced. *B*, calcium waves, channel and bursting activities in cultured preBötC neurons at 16 DIV, which showed no spontaneous activity in the standard ACSF containing 3 mM $[K^+]_o$. Top left, propagating $[Ca^{2+}]_i$ wave triggered by a puff of high-K^+ solution onto the left neuron in the inset (the temporal and spatial widths of the application spot were 0.1 s and 5 μm, respectively). The wave speed (71 μm s^{-1}) was obtained from the calcium profiles measured along the white line in the DIC image (the arrows indicate the locations of peaks). Lower pairs of traces were recorded 1 min after addition of 10 μM CNQX (AMPAR antagonist) to the bath. Note that although in this case $[Ca^{2+}]_i$ showed increase near the stimulation site, the transient did not propagate. The right panel shows activation of TRPM4-like channels and burst of action potentials due to stimulation. The rightmost trace was obtained after elevating bath $[K^+]_o$ to 7 mM, after which spontaneous transients appeared and they were similar to the evoked responses. *C*, calcium waves induced by local depolarization of distant dendrite. DIC image in the inset shows the positions of stimulation and perfusion pipettes. Calculated wave speed, 70 μm s^{-1}. Application of thapsigargin (Tg, 1 μM) in the middle of dendrite locally elevated calcium, that inhibited wave propagation. After washing out thapsigargin, $[K^+]_o$ was increased from 3 to 7 mM, that induced spontaneous $[Ca^{2+}]_i$ spikes which spread out in the dendrite at a velocity of 67 μm s^{-1}. Scale bars in all panels, 20 μm.

of the velocity of calcium waves supported by CICR (Mironova & Mironov, 2008). When calcium waves crossed the soma, the activity of TRPM4-like channels transiently increased. P_{open}/N increased from 0.21 ± 0.04 to 0.42 ± 0.06 ($P < 0.05$; $n = 6$) and the peak of channel activity coincided with the beginning of bursting activity. Bath application of 5 μM DHPG for 2 min increased wave velocity to $\sim$100 μm s^{-1}, shortened the time interval (latency) between the initiation of the wave and burst generation by 63 ± 7% and prolonged the burst duration by 54 ± 6% ($P < 0.05$, $n = 5$). In the presence of 300 μM flufenamate, the wave velocity was close to that measured in the control, but the burst was suppressed (Fig. 6*A*, $n = 4$).

Generation and propagation of calcium waves in cultured preBötC neurons

Neurons in primary culture also showed spontaneous calcium waves and, when absent, they can be evoked by membrane depolarization, using a brief puff of 45 mM K^+. Spontaneous waves occurred more frequently in 'young' preparations (cultures younger than 7 DIV). This is similar to the finding in other neuronal cultures, where such waves are implicated in the development of synapses (Spitzer *et al.* 2002). We examined the waves in cultures older that 7 DIV, where spontaneous activity was absent (Supplement 2). Selecting a pair of neurons, we stimulated one cell that produced the calcium wave that propagated to the second cell. Upon its arrival at the soma, the activity of TRPM-like channels was enhanced which was followed by the burst of action potentials (Fig. 6*B*, the first row of traces). In the presence of CNQX, the blocker of AMPA/kainate receptors, the initial Ca^{2+} spike was attenuated, it did not propagate and the activity of TRPM4-like channels showed no specific changes ($n = 4$, Fig. 6*B*). The effects of CNQX indicate that AMPA receptor-mediated depolarizations are essential in promoting the initial Ca^{2+} flux needed for the activation of CICR mechanism during wave propagation. Both spontaneous calcium waves and 'inspiratory' bursts were established after elevation of $[K^+]_o$ from 3 to 7 mM (Fig. 6*C*, the right-most trace).

Calcium waves were also evoked by stimulation of distant dendrites (Fig. 6*C*). In order to test the involvement of CICR, we applied thapsigargin in the middle of the dendrite, that interrupted the waves. Spontaneous calcium waves appeared after elevation of $[K^+]_o$ to 7 mM (the right-most couple of traces in Fig. 6*C*). They were first seen in distant dendrites and then spread out to the soma with about the same velocity as the waves which were evoked by membrane depolarization.

Calcium spikes and waves '*in silico*'

Correlation between calcium waves and bursting activity prompted us to examine the issue of whether such waves can produce emerging activity in a network. Since neurons in the respiratory network often formed clusters (Fig. 4, see also Hartelt *et al.* 2008), we first asked whether the calcium waves can synchronize the electrical activity of neurons in clusters. We considered an array of 'excitability' sites and positioned the neurons between them. Each site was capable of generating calcium transients and the time-dependent calcium changes in each neuron were translated into V_m changes through activation of TRPM4-like conductance (see Methods for details). Figure 7*A* presents the results of simulations for a ring consisting of eight neurons (the results of simulations were similar for other configurations examined). It is seen that initially random transients quickly synchronized and they produced either low- or high-frequency patterns of activity, whose appearance depended on the delay assumed for the wave propagation within a cluster. For delays < 1 s, all neurons showed simultaneous depolarizations at frequencies 7–8 peaks min^{-1} (Fig. 7*A*, Supplementary Movie 5), that was close to that of the frequency of respiratory motor output in the functional slice preparation (Figs 2–4). For delays > 2 s, the frequency was significantly higher (20–40 peaks min^{-1}). In this case, the neurons were depolarized one after another (Supplementary Movie 6). For intermediate delays, both low- and high-frequency patterns were observed (the middle trace in Fig. 7*A*) which may represent complex types of behaviour such as produced in other types of networks as described in books of Kuramoto (2003), Strogatz (2004) and Newman *et al.* (2006). Full analysis of activities generated within this model will be presented elsewhere. The main conclusion gained from simulations and which is relevant to the present study is that simultaneous discharges of neurons in cluster are established for short (< 1 s) delays in interactions between neurons.

In order to produce persistent oscillatory activity, the discharges of neuronal clusters must be synchronized. We modelled this situation by considering the clusters (within each the cells discharged simultaneously) which communicated via the calcium waves. In the representative case shown in the inset in Fig. 7*B*, the clusters were assumed to interact by using only one connection between excitability sites, but the conclusions reached were not affected by this assumption. It appeared that, independently of the interaction delay, the population activity was always synchronized at an intrinsic oscillation frequency of about 7 peaks min^{-1} (Fig. 7*B*). This indicates that separations between clusters are seemingly less critical for synchronization between clusters than the establishment of oscillatory activity within a cluster. Hierarchical organization of neurons in the network is in line with the topology of the respiratory network (Hartelt *et al.* 2008) and it may be beneficial for maintaining the function, when some network elements fail.

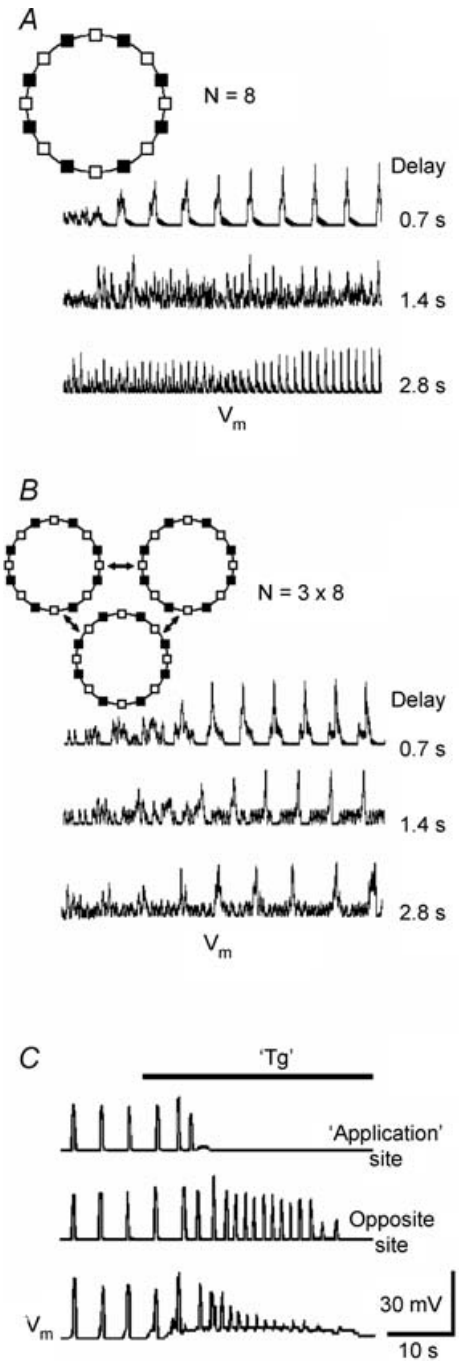

Figure 7. Modelling
Simulations were performed using the model described in Methods. The insets in *A* and *B* show configurations used. They included excitability sites (empty squares), which were connected with each other and to the neurons (filled squares). Delays in the propagation of calcium waves between the sites are given near each trace. In neurons, calcium elevations activated TRPM4-like channels that produced suprathreshold membrane depolarizations. Population activities were calculated as mean voltage within a cluster. *A* and *B* show representative simulations for a ring of eight neurons and three interconnected rings, respectively. *C* shows the effects of local application of thapsigargin (TG) to one site in the ring of eight neurons (delay, 0.7 s). The activity was first enhanced due to Ca^{2+} release from ER and then subsided after its depletion.

Finally, we modelled the results of experiments with inhibition of cluster activity by thapsigargin (Fig. 4*B*). When it was 'added' locally to one 'excitability' site, it produced Ca^{2+} release at the 'application' site that first caused transient potentiation of the activity of all neurons within a cluster, after which it subsided, when the 'ER' was emptied. These results reproduce well the experimental data shown in Fig. 4*B*.

Discussion

Using two-photon calcium imaging of the functional slice preparation and patch-clamp recordings of targeted cells, we examined the spatiotemporal dynamics of spontaneous activity in the respiratory network. It exhibited characteristic patterns of synchronous activity as indicated by simultaneous calcium elevations in coactive ensembles dispersed throughout the slice. We observed synchronous activity in small clusters of neurons. Such organization possibly reflects a topology of the respiratory network (Hartelt *et al.* 2008) and implies a geometrical basis for a group-pacemaker hypothesis (Feldman & Del Negro, 2006).

Examination of neuronal activity in clusters revealed a concerted interplay between metabotropic glutamate receptors, calcium waves in dendrites and calcium-activated non-selective channels. On the basis of data obtained, we propose the following steps, which can drive the emerging activity in a network: (i) activation of mGluR in dendrites initiates calcium waves which spread out towards the soma; and (ii) resulting $[Ca^{2+}]_i$ elevations activate TRPM4-like channels and lead to membrane depolarization and generation of inspiratory bursts. These suggestions are congruent with a group-pacemaker hypothesis (Feldman & Del Negro, 2006), which assumes that the respiratory network cycles between the two main states: (1) the refractory state that follows inspiration, in which excitatory synapses in the network are inactive (this corresponds to the absence of calcium waves within clusters); and (2) the short-lived active state, where a positive-feedback process leads to aggregation of the network (calcium waves circulate within clusters). Calcium waves observed in dendrites of inspiratory neurons use a regenerative mechanism of Ca^{2+}-induced Ca^{2+} release for activation (a positive feedback) and have intrinsic refractoriness, which is determined by the Ca^{2+}-dependent inactivation (desensitization) of Ca^{2+} release channels that can last several seconds. The modelling shows that calcium waves are able to synchronize the activity of neurons within a cluster and between them (Fig. 7). Glutamatergic synaptic transmission (Rekling & Feldman, 1998; Richter & Spyer, 2001; Feldman & Del Negro, 2006) is also important in synchronization of activity between the clusters. Glutamatergic synapses and calcium waves

are closely related and can synergetically enhance each other. For example, depolarization due to activation of AMPA/kainate receptors increases Ca^{2+} influx that can facilitate Ca^{2+} release from ER and propagating calcium waves can enhance the release of glutamate.

Theoretical models of neuronal networks are usually based on one of three models: the Kuramoto model (2003), which considers global coupling of all oscillators; the Strogatz–Watts small-world network (Strogatz, 2004), and scale-free or 'richer-gets-rich' model of Barabási-Albert (Newman *et al.* 2006), which assumes that new connections are more easily formed by neurons already having more connections. The topology of the respiratory network (Hartelt *et al.* 2008) resembles a small-world network, but much work is still needed to combine this spatial organization of the network with its function, to elucidate the role of respiratory neurons with different functional properties, and to account for the effects of other brainstem regions.

During the last decade intense research was done in the study of transient receptor potential (TRP) channels (see Wissenbach *et al.* 2004; Kraft & Harteneck, 2005; Ramsey *et al.* 2006; Nilius *et al.* 2007 for some recent reviews). Less is known about the role of these channels in the respiratory network. Crowder *et al.* (2007) showed that TRPM4/5 channels are expressed in preBötC and proposed their important role in generation of the inspiratory bursts. We characterized single channels in the inspiratory neurons (Fig. 3) and showed that the channels are non-selective (E_{rev} ~0 mV), have unitary conductance 24 pS, are voltage dependent and show outward rectification. The channels were activated by intracellular Ca^{2+} and PIP_2, and were inhibited by flufenamate, Gd^{3+} and ATP. The properties of TRPM4 and TRPM5 channels are similar, but there are also certain differences (Kraft & Harteneck, 2005). For example, TRPM4 channels are more sensitive to flufenamate ($EC_{50} = 3\ \mu$M *versus* 24 μM for TRPM5) and to ATP^{4-} (half-block at 1 μM, whereas TRPM5 channels are not inhibited up to 1 mM, Nilius *et al.* 2005). Activation of TRPM5 channels by Ca^{2+} corresponds to a bell-shaped curve which has a maximum at about 1 μM, and at 10 μM the activity disappears, whereas TRPM4 channels are activated according to $EC_{50} \approx 1\ \mu$M and show no Ca^{2+}-dependent desensitization (Prawitt *et al.* 2003). This disagrees with previous indications of much higher EC_{50} values of 10–20 μM for TRPM4 channels (reviewed in Kraft & Harteneck, 2005). The discrepancies have been recently explained by Nilius *et al.* (2005) who found that the Ca^{2+} sensitivity of TRPM4 channels is regulated by ATP, PKC-dependent phosphorylation, and calmodulin binding at the C terminus and can therefore be different under various experimental conditions. Such plasticity of TRPM4 channels can also accomplish a variety of control mechanisms of neural bursting activity. The fact that TRPM4 channels were blocked in the inside-out patches by 10 μM flufenamate and 19 μM ATP^{4-}, and are fully activated by 10 μM Ca^{2+}, suggests that we recorded TRPM4-like channels. It is important to learn more about their expression patterns in respiratory neurons, coupling to various intracellular signalling pathways, developmental pattern and possible role in respiratory diseases.

Beyond TRPM4-like channels, other channels such as persistent Na^+ (Butera *et al.* 1999), voltage-dependent Ca^{2+} and Ca^{2+}-dependent K^+ (Onimaru *et al.* 2003; Busselberg *et al.* 2003) may play an important role in shaping respiratory activity. A recently described novel channel NACLN (Lu *et al.* 2007) also deserves attention. Its direct involvement in the generation of oscillator activity is unlikely, because the channel is voltage- and time-independent. Perhaps this channel is important in pre-depolarization of the respiratory neurons, whereby they acquire the ability to generate the bursts. If NACLN channels are differentially expressed in the respiratory network, this could explain the functional differences observed between various types of neurons active in the preBötC (Rekling & Feldman, 1998; Richter & Spyer, 2001). As suggested by an anonymous reviewer, a subset of neurons (within or outside the preBötC) which express NACLN can be tonically active and project to rhythmogenic neurons to start the calcium waves.

Communication between metabotropic (mGluR1/5) and ionotropic (TRPM4) receptors mediated by calcium waves has been previously noticed in other neurons. The calcium waves observed here in the functional brainstem preparation were similar to those described in hippocampal and cortical neurons (Larkum *et al.* 2003; Hagenston *et al*. 2008), where they are generated by mGluR1/5 and regulate neuronal firing. Loewenstein & Sompolinsky (2003) proposed that calcium waves in dendrites can be used to transmit information from dendrites to the soma and backwards. Our model of the neural network suggests that dendritic calcium waves can synchronize the activity of neurons in small formations (clusters). It may find implications in other networks such as in cortex and thalamus, where the neurons demonstrate a large-scale synchrony.

References

Augustine GJ, Santamaria F & Tanaka K (2003). Local calcium signaling in neurons. *Neuron* **40**, 331–346.

Baker RE, Ballantyne D, Bingmann D, Jones D & Widman G (1995). Rhythm generation in medullary cultures of newborn rats. *Int J Dev Neurosci* **13**, 799–809.

Busselberg D, Bischoff AM & Richter DW (2003). A combined blockade of glycine and Ca^{2+}-dependent K^+ channels abolishes respiratory rhythm. *Neuroscience* **122**, 831–841.

Butera RJ, Rinzel J & Smith JC (1999). Models of respiratory rhythm generation in the pre-Botzinger complex. I. Bursting pacemaker neurons. *J Neurophysiol* **82**, 382–397.

Campbell CG, Spray DC & Wolkoff AW (1993). Extracellular ATP^{4-} modulates organic anion transport by rat hepatocytes. *J Biol Chem* **268**, 15399–15404.

Cho H, Kim MS, Shim WS, Yang YD, Koo J & Oh U (2003). Calcium-activated cationic channel in rat sensory neurons. *Eur J Neurosci* **17**, 2630–2638.

Crowder EA, Saha MS, Pace RW, Zhang H, Prestwich GD & Del Negro CA (2007). Phosphatidylinositol 4,5-bisphosphate regulates inspiratory burst activity in the neonatal mouse preBötzinger complex. *J Physiol* **582**, 1047–1058.

Del Negro CA, Morgado-Valle C & Feldman JL (2002). Respiratory rhythm: an emergent network property? *Neuron* **34**, 821–830.

Feldman JL & Del Negro CA (2006). Looking for inspiration: new perspectives on respiratory rhythm. *Nat Rev Neurosci* **7**, 232–242.

Gray PA, Rekling JC, Bocchiaro CM & Feldman JL (1999). Normal breathing requires preBotzinger complex neurokinin-1 receptor-expressing neurons. *Science* **286**, 1566–1568.

Guyenet PG & Wang H (2001). Pre-Bötzinger neurons with preinspiratory discharges 'in vivo' express NK1 receptors in the rat. *J Neurophysiol* **86**, 438–446.

Hagenston AM, Fitzpatrick JS & Yeckel1 MF (2008). MGluR-mediated calcium waves that invade the soma regulate firing in layer V medial prefrontal cortical pyramidal neurons. *Cereb Cortex* **18**, 407–423.

Haller M, Mironov SL, Karschin A & Richter DW (2001). Dynamic activation of K_{ATP} channels in rhythmically active neurons. *J Physiol* **537**, 69–81.

Hamill OP & McBride DW (1996). The pharmacology of mechano-gated membrane ion channels. *Pharmacol Rev* **48**, 231–252.

Hartelt N, Skorova E, Manzke T, Suhr M, Mironova LA, Kügler S & Mironov SL (2008). Imaging of respiratory network topology in living brainstem slices. *Mol Cell Neurosci* **37**, 425–431.

Koshiya N & Smith JC (1999). Neuronal pacemaker for breathing visualized in vitro. *Nature* **400**, 360–363.

Kraft R & Harteneck C (2005). The mammalian melastatin-related transient receptor potential cation channels: an overview. *Pflugers Arch* **451**, 204–211.

Kuramoto Y (2003). *Chemical Oscillations, Waves, and Turbulence*. Dover Publications, London.

Larkum ME, Watanabe S, Nakamura T, Lasser-Ross N & Ross WN (2003). Synaptically activated Ca^{2+} waves in layer 2/3 and layer 5 rat neocortical pyramidal neurons. *J Physiol* **549**, 471–488.

Loewenstein Y & Sompolinsky H (2003). Temporal integration by calcium dynamics in a model neuron. *Nat Neurosci* **6**, 961–967.

Lu B, Su Y, Das S, Liu J, Xia J & Ren D (2007). The neuronal channel NALCN contributes resting sodium permeability and is required for normal respiratory rhythm. *Cell* **129**, 371–383.

McKay LC, Janczewski WA & Feldman JL (2005). Sleep-disordered breathing after targeted ablation of preBötzinger complex neurons. *Nat Neurosci* **8**, 1142–1144.

Manzke T, Guenther U, Ponimaskin EG, Haller M, Dutschmann M, Schwarzacher S & Richter DW (2003). $5\text{-}HT4_a$ receptors avert opioid-induced breathing depression without loss of analgesia. *Science* **301**, 226–229.

Mironov SL (1983). Theoretical model of slow-wave membrane potential oscillations in molluscan neurons. *Neuroscience* **10**, 899–905.

Mironov SL (1990). Theoretical analysis of calcium wave propagation along the surface of intracellular stores. *J Theor Biol* **59**, 403–411.

Mironov SL (1994). Mechanisms of Ca^{2+} mobilization in chick sensory neurones. *Neuroreport* **12**, 445–448.

Mironov SL (2006). Spontaneous and evoked neuronal activities regulate movements of single neuronal mitochondria. *Synapse* **59**, 403–411.

Mironov SL & Langohr K (2005). Mechanisms of Na^+ and Ca^{2+} influx into respiratory neurons during hypoxia. *Neuropharmacology* **48**, 1056–1065.

Mironov SL, Langohr K, Haller M & Richter DW (1998). Hypoxia activates ATP-dependent potassium channels in inspiratory neurones of neonatal mice. *J Physiol* **509**, 755–766.

Mironov SL, Langohr K & Richter DW (2000). Hyperpolarization-activated current, I_h, in inspiratory brainstem neurons and its inhibition by hypoxia. *Eur J Neurosci* **12**, 520–526.

Mironov SL & Richter DW (2000*a*). Intracellular signalling pathways modulate K_{ATP} channels in inspiratory brainstem neurones and their hypoxic activation: Involvement of metabotropic receptors, G-proteins and cytoskeleton. *Brain Res* **853**, 60–67.

Mironov SL & Richter DW (2000*b*). Modulation of L-type Ca channels in inspiratory brainstem neurones: Intracellular signalling pathways and metabotropic glutamate receptors. *Brain Res* **869**, 166–177.

Mironov SL & Symonchuk N (2006). ER vesicles and mitochondria move and communicate at synapses. *J Cell Sci* **119**, 4926–4934.

Mironov SL, Usachev YM & Lux HD (1993). Spatial and temporal control of intracellular free Ca^{2+} in chick sensory neurons. *Pflugers Arch* **424**, 183–191.

Mironova LA & Mironov SL (2008). Approximate analytical time-dependent solutions to describe large-amplitude local calcium transients in the presence of buffers. *Biophys J* **94**, 349–358.

Morita H, Honda A, Inoue R, Ito Y, Abe K, Nelson MT & Brayden JE (2007). Membrane stretch-induced activation of a TRPM4-like nonselective cation channel in cerebral artery myocytes. *J Pharmacol Sci* **103**, 417–426.

Müller M, Schmidt J, Mironov SL & Richter DW (2003). Construction and performance of a custom-built 2-photon laser scanning system. *J Phys D: Appl. Phys* **36**, 1747–1757.

Newman M, Watts D & Barabási AL (2006). *The Structure and Dynamics of Networks*. Princeton University Press. Princeton.

Nilius B, Owsianik G, Voets T & Peters JA (2007). Transient receptor potential cation channels in disease. *Physiol Rev* **87**, 165–217.

Nilius B, Prenen J, Tang J, Wang C, Owsianik G, Janssens A, Voets T & Zhu MX (2005). Regulation of the Ca^{2+} sensitivity of the nonselective cation channel TRPM4. *J Biol Chem* **280**, 6423–6433.

Nistri A, Ostroumov K, Sharifullina E & Taccola G (2006). Tuning and playing a motor rhythm: how metabotropic glutamate receptors orchestrate generation of motor patterns in the mammalian central nervous system. *J Physiol* **572**, 323–334.

Onimaru H, Ballanyi K & Homma I (2003). Contribution of Ca^{2+}-dependent conductances to membrane potential fluctuations of medullary respiratory neurons of newborn rats *in vitro*. *J Physiol* **552**, 727–741.

Pace RW, Mackay DD, Feldman JL & Del Negro CA (2007). Inspiratory bursts in the preBötzinger complex depend on a calcium-activated non-specific cation current linked to glutamate receptors in neonatal mice. *J Physiol* **582**, 113–125.

Prawitt D, Monteilh-Zoller MK, Brixel L, Spangenberg C, Zabel B, Fleig A & Penner R (2003). TRPM is a transient Ca^{2+}-activated cation channel responding to rapid changes in $[Ca^{2+}]_i$. *Proc Natl Acad Sci U S A* **100**, 15166–15171.

Ramsey IS, Delling M & Clapham DE (2006). Introduction to TRP channels. *Annu Rev Physiol* **68**, 619–647.

Rekling JC & Feldman JL (1998). Pre-Bötzinger complex and pacemaker neurons: Hypothesized site for respiratory rhythm generation. *Ann Rev Physiol* **60**, 385–405.

Richter DW & Spyer KM (2001). Studying rhythmogenesis of breathing: comparison of in vivo and in vitro models. *Trends Neurosci* **24**, 464–472.

Ruangkittisakul A, Schwarzacher SW, Secchia L, Poon BY, Ma Y, Funk GD & Ballanyi K (2006). High sensitivity to neuromodulator-activated signaling pathways at physiological $[K^+]$ of confocally imaged respiratory center neurons in on-line-calibrated newborn rat brainstem slices. *J Neurosci* **26**, 11870–11880.

Spitzer NC, Kingston PA, Manning TJ & Conklin MW (2002). Outside and in: development of neuronal excitability. *Curr Opin Neurobiol* **12**, 315–323.

Strogatz S (2004). *Sync: the Emerging Science of Spontaneous Order*. Penguin Press Science, London.

Thoby-Brisson M, Cauli B, Champagnat J, Fortin G & Katz DM (2003). Expression of functional tyrosine kinase B receptors by rhythmically active respiratory neurons in the pre-Bötzinger complex of neonatal mice. *J Neurosci* **23**, 7685–7689.

Thoby-Brisson M, Trinh J, Champagnat J & Fortin G (2005). Emergence of pre-Bötzinger respiratory rhythm generator in the mouse embryo. *J Neurosci* **25**, 4307–4318.

Wissenbach U, Niemeyer BA & Flockerzi V (2004). TRP channels as potential drug targets. *Biol Cell* **96**, 47–54.

Acknowledgements

The author would like to thank N. Hartelt and K. Langohr for the preparation of functional slices, J. Schmidt for the help with a two-photon microscope, T. Szellas and T. Manzke for the help in immunocytochemistry, and C. Maggs for reading the manuscript and helpful comments.

Supplemental material

Online supplemental material for this paper can be accessed at:
http://jp.physoc.org/cgi/content/full/jphysiol.2007.149021/DC1
and
http://www.blackwell-synergy.com/doi/suppl/10.1113/jphysiol.2007.149021